ISSN (Print) 1226-1750
ISSN (Online) 2233-6656
Journal of Magnetics 18(4), 391-394 (2013) http://dx.doi.org/10.4283/JMAG.2013.18.4.391

Effect of Copper Substitution on Structural and Magnetic Properties of NiZn Ferrite Nanopowders

Mohammad Niyaifar*, Hoda Shalilian, Ahmad Hasanpour, and Hory Mohammadpour

Department of Physics, Science and Research Branch, Islamic Azad University, Khouzestan, Iran

(Received 23 June 2013, Received in final form 7 October 2013, Accepted 9 October 2013)

In this study, nickel-zinc ferrite nanoparticles, with the chemical formula of $Ni_{0.3}Zn_{0.7-x}Cu_xFe_2O_4$ (where x = 0.1-0.6 by step 0.1), were fabricated by the sol-gel method. The effect of copper substitution on the phase formation and crystal structure of the sample was investigated by X-ray diffraction (XRD), thermo-gravimetry (TG), differential thermal analysis (DTA), Fourier transform infrared spectrometry (FT-IR), scanning electron microscopy (SEM) and transmission electron microscopy (TEM). The XRD result shows that due to the reduction of Zn content,the crystallite size of the sample increased. The results of the vibration sample magnetometer (VSM) exhibit an increase in saturation magnetization value (Ms) for samples with $x \leq 0.3$ and a linear decrease for samples with $x > 0.3$. The variation of saturation magnetization and coercivity of the samples were then studied.

Keywords : Cu substituted nickel-zinc ferrite, sol-gel, magnetic properties

1. Introduction

Ferrites are a class of spinel oxide which is technically very important [1-4]. The general formula is MFe_2O_4, in which M is one or a combination of divalent ions. From a crystallography perspective, the structure of bulk nickel-zinc ferrite is shown in Eq. (1):

$$(Zn^{2+}_{1-z}Fe^{3+}_{1-y})[Ni^{2+}_{z}Fe^{3+}_{1-y}]O^{2-}_{4} \quad (1)$$

The cations inside the parentheses occupy tetrahedral sublattice (A) and those inside the brackets occupy octahedral sublattice (B). One of the magnetic parameters which play a crucial rule in the magnetic properties of ferrites is permeability. In general, the maximum value of nickel zinc ferrite permeability can be obtained in three different ways: providing Fe^{3+} ions [5], setting zinc content (z) at 0.7 [2], and substitution of copper ions (Cu^{2+}) in nickel zinc ferrite [6].The other benefit of the copper ion substitution in zinc nickel ferrite is the prevention of the magnetic losses (energy losses) that cause a transition in the structural phase [7]. This transition is accompanied by a reduction of the crystal symmetry that occurs as a result of the Jahn-Teller effect [8]. In this study, samples were synthesized via the sol-gel method by using polyvinyl alcohol as a chelating agent, because of its properties including high polarity and resistance to aqueous solvents. The structure, morphology, and magnetic properties of the samples were investigated.

2. Experimental

NiZnCu ferrite, with the chemical composition of $Ni_{0.3}Zn_{0.7-x}Cu_xFe_2O_4$ where $0.1 \leq x \leq 0.6$, was prepared by the sol-gel method using nickel nitrate (Ni $(NO_3)_2 \cdot 6H_2O$), zinc nitrate (Zn $(NO_3)_2 \cdot 6H_2O$), copper nitrate (Cu $(NO_3)_2 \cdot 3H_2O$, and iron nitrate (Fe $(NO_3)_3 \cdot 9H_2O$). The nitrates were weighted according to the required stoichiometric proportion and dissolved in deionized water. Polyvinyl alcohol (PVA) was then added to the solution. The molar ratio of total metal ions to PVA was maintained to be 1:2. With continuous stirring at 70°C, the PVA was dissolved so that the brown sol was formed. The resulting sol was heated at 90 °C for 24 h to obtain dried gel. The dried gel was then annealed at 1000 °C for 2 h.

3. Results and Discussion

3.1. Thermal Decomposition characterization

Figure 1 shows a typical TG and DTA curve of the

*Corresponding author: Tel: +98 9351055293
Fax: +98 611 4457612, e-mail: md.niyaifar@gmail.com

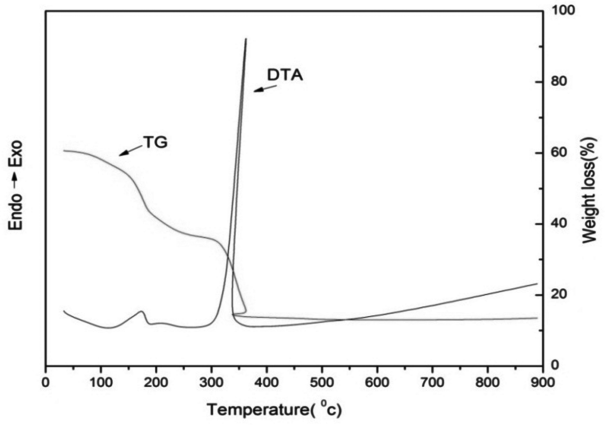

Fig. 1. DTA and TG plots of the dried gel of $Ni_{0.3}Zn_{0.6}Cu_{0.1}Fe_2O_4$.

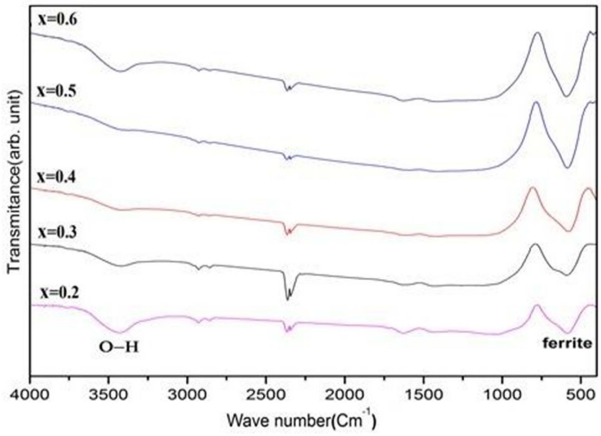

Fig. 3. (Color online) IR spectra of $Ni_{0.3}Zn_{0.7-x}Cu_xFe_2O_4$ nanopowders calcined at 1000 °C.

dried gels. From the TG curve, three parts are estimated: weight loss, endothermic peak, and two exothermic peaks. The first step of weight loss occurs in the thermal range of 52.25-165 °C, which is associated with an endothermic peak of 172.19 °C in the DTA curve; this endothermic peak is related to the loss of dried gel humidity physically and chemically. The second step occurs in the thermal range of 165-285.71 °C, due to the decomposition of nitrates in the dried gel. The sharp endothermic peak of 362.32 °C in the DTA curve depends on the crystallization of the spinel structure of the copper zinc nickel ferrite [1, 9]. At a temperature higher than 362.32 °C, no weight reduction is observed, which suggests that the thermal process has not yet been completed.

3.2. Structural characterization

Figure 2 shows the X-ray diffraction pattern of the samples. It can be seen that the powders possess a pure cubic spinel structure. The average crystallite sizes of samples were determined using Scherer's formula (Table 1). Crystallite size grows by increasing the Cu content. The growth of crystallites can be attributed to the reduction of zinc content, which can be explained by the effect of surface temperature on the molecular concentration at the surface of the crystal [12]. The formation of zinc ferrite is more exothermic ($\Delta H_{ZnFe_2O_4}$ = –2.68 Kcal/mole) than that of copper ferrite ($\Delta H_{CuFe_2O_4}$ =5.05 Kcal/mole) [13]. Thus, it is expected that less heat will be liberated by decreasing the zinc content in the system. This increases the molecular concentration at the crystal surface and hence the growth of the grains [12, 14]. Also, the lattice constant increases linearly with the copper ratio, which can be attributed to a larger copper ionic radius (0.87 Å) compared to the zinc ionic radius (0.74 Å) (Table 1) [15].

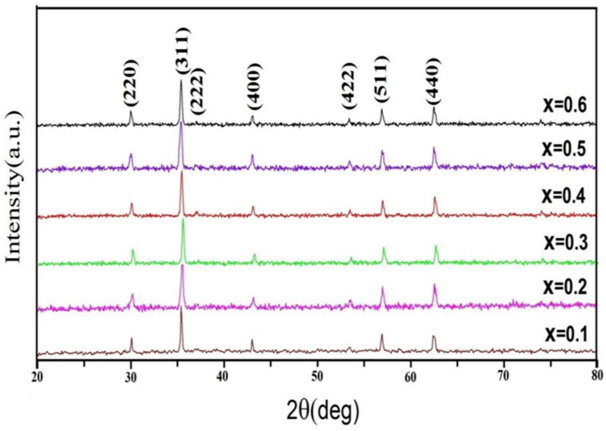

Fig. 2. (Color online) Characteristic parts of XRD patterns of $Ni_{0.3}Zn_{0.7-x}Cu_xFe_2O_4$.

3.3. FT-IR analysis

Figure 3 shows the FT-IR spectra of the samples. With respect to ferrite structures, the most prominent part of IR is in the 800-250 cm^{-1} range [10]. This range is assigned to the vibration of metal-oxygen bands in octahedral sites.

Table 1. Lattice parameter, crystalline, and particle size calculated from XRD spectra of $Ni_{0.3}Zn_{0.7-x}CuxFe_2O_4$nanopowders calcined at 1000 °C for 2 h.

Particle size (nm)	Crystalline size (nm)	Lattice constant (Å)	Cucontent (x)
87	21	8.399	0.1
114	28	8.401	0.2
120	29	8.409	0.3
134	39	8.414	0.4
146	40	8.418	0.5
168	43	8.420	0.6

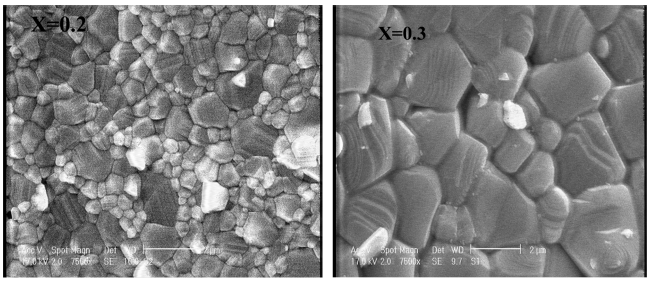

Fig. 4. SEM image of $Ni_{0.3}Zn_{0.7-x}Cu_xFe_2O_4$ (x = 0.2 and 0.3) nanopowders annealed at 1000 °C.

However, in our spectra, only a stretching vibration in the tetrahedral site can be observed. From the FT-IR spectra, the existence of a slight shift can be seen for the tetrahedral absorption peak towards the higher wave number with u substitution. Such shifts indicate changes in the metal-oxygen bands and also the effect of atomic weight due to substitution [11].

The electron scanning microscope (Fig. 4) shows that the increase of copper substitution has no significant effect on the morphology of the samples. However, this substitution increases the average grain size from 87 to 168 nm.

3.4. Magnetic measurements

Figure 5 shows the magnetic hysteresis loops of the samples measured at room temperature. It can be seen that saturation magnetization increases with copper content up to x = 0.3 and then decreases for x > 0.3 (Fig. 3(a)). The behavior of the saturation magnetization can be explained on the basis of cations distribution and super-exchange interactions. A recent study shows that zinc ferrite and nickel ferrite over 50 nm have normal spinel and inverse spinel structures, respectively [16-18]. Moreover, $CuFe_2O_4$ is known to be largely an inverse spinel, which is confirmed by Mossbauer measurements in an applied magnetic field [19]. Therefore, by substitution of copper ions in nickel-zinc ferrite, Cu^{+2} ions occupy the octahedral sites, so the cation distribution of the samples can be expected as Eq. (2).

$$(Zn^{2+}_{0.7-x}Fe^{+3}_{0.3+x})_A[Ni^{2+}_{0.3}Cu^{2+}_{x}Fe^{+3}_{1.7-x}]_BO^{-4} \quad (2)$$

According to Eq. (2), the increase of magnetic Cu^{+2} ions (1.73 μ_B) [20] in the octahedral site and the migration of the same amount of Fe^{+3} ions (5 μ_B) from the octahedral to the tetrahedral sites causes an increase in superexchange interaction for all samples. The increase of the superexchange interaction decreases the spin canting in both sublattices, and consequently the Neel's collinear arrangement

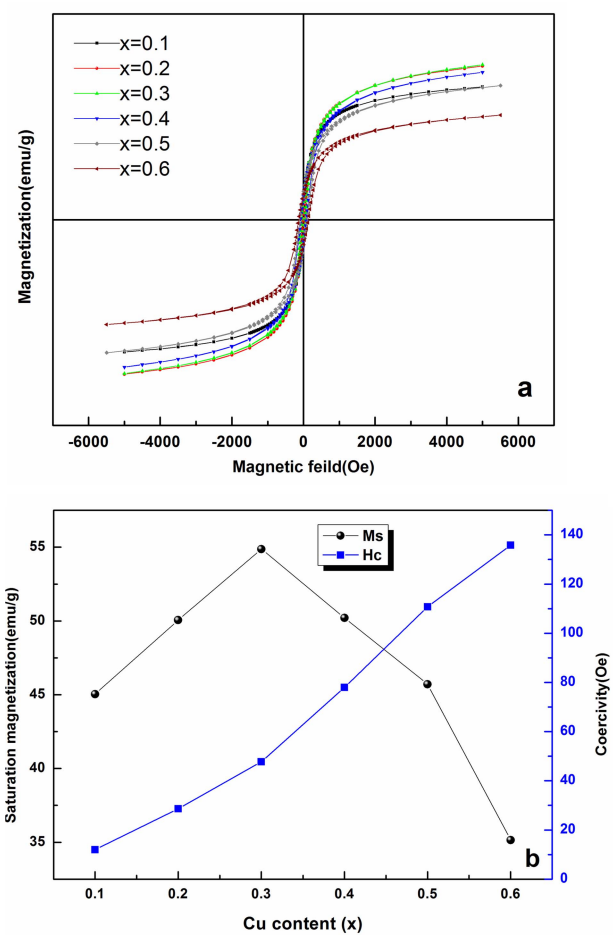

Fig. 5. (Color online) (a) Magnetic hysteresis loops of $Ni_{0.3}Zn_{0.7-x}Cu_xFe_2O_4$ samples and (b) variation of saturation magnetization and the coercivity with the Cu content.

shows its effect at a higher concentration of Cu^{+2} ions. The observed increase in saturation magnetization for samples with x ≤ 0.3 can therefore be attributed to increases of the A-B superexchange interaction. Thereafter, the decrease of saturation magnetization for samples with x > 0.3 can be explained by the anti-parallel alignment effect on the basis of Neel's model (Fig. 3(b)). With the increase of copper substitution, the magnetic coercivity of samples increases. It is well known that Cu^{+2} ions have more magneto-crystalline anisotropy than Zn^{+2} ions [21]. The observed increase in coercivity can therefore be attributed to the increase of Cu content.

4. Conclusions

In summary, copper zinc nickel ferrites were prepared by the sol-gel method using polyvinyl alcohol. The average crystallite size was increased from 21 to 43 nm. This increase is attributed to the reduction of zinc content. The

variation of the saturation magnetization of the samples was explained on the basis of superexchange interaction and Neel's model. Also, the observed increase in coercivity values is attributed to the increase of magneto-crystalline anisotropy.

References

[1] S. Yan, J. Yin, and E. Zhou, J. Alloys Compd. **450**, 417 (2008).
[2] H.-W. Wang and S.-C. Kung, J. Magn. Magn. Mater. **270**, 230 (2004).
[3] C. S. Kim, W. C. Kim, S. Y. An, and S. W. Lee, J. Magn. Magn. Mater. **215-216**, 213 (2000).
[4] B. P. Rao, A. M. Kumar, K. H. Rao, Y. L. N. Murthya, O. F. Caltun, I. Dumitruc, and L. Spinuc, J. Optoelectron. Adv. Mater. **8**, 1703 (2006).
[5] J. Hu and Y. Mi, J. Zhejiang Univ. Sci. B. **6**, 580 (2005).
[6] M. Usakova, J. Luka, R. Dosoudil, V. Jancarik, A. Gruskova, E. Usak, J. Slama, and J. Subrt, J. Mater. Sci.-Mater. Electron. **18**, 1183 (2007).
[7] J. Bera and P. K. Roy, J. Mater. Process. Technol. **197**, 279 (2008).
[8] S. Zahi, M. Hashim, and A. R. Duad, Mater. Lett. **60**, 2803 (2006).
[9] Yu. Liming, Sh. Cao, Y. Liu, J. Wang, Ch. Jing, and J. Zhang, J.Magn. Magn. Mater. **301**, 100 (2006).
[10] R. D. Waldron, Phys. Rev. **99**, 1727 (1955).
[11] M. Reichenbächer and J. Popp, Springer-Verlag, Berlin Heidelberg (2012).
[12] C. Upadhyay, H. C. Verma, and S. Anand, J. Appl. Phys. **95**, 5746 (2004).
[13] A. Navrotsky and O. J. Kleppa, J. Inorg, Nucl. Chem. **30**, 479 (1968).
[14] I. H. Gul, W. Ahmed, and A. Maqsood, J. Magn. Magn. Mater. **320**, 270 (2008).
[15] Z. Yue, L. Li, J. Zhou, H. Zhang, and Z. Gui, Mater. Sci. Eng., B **64**, 68 (1999).
[16] M. Atif, S. K. Hasanain, and M. Nadeem, Solid State Commun. **138**, 416 (2006).
[17] J. Jacob and M. Abdul Khadar, J. Appl. Phys. **107**, 114310 (2010).
[18] D.-H. Chen and X.-R. He, Mater. Res. Bull. **36**, 1369 (2001).
[19] V. U. Patil and R. G. Kulkarni, Solid State Commun. **31**, 551 (1979).
[20] A. A. Samokhvalov, T. I. Arbuzova, N. A.Viglin, V. V. Osipov, N. I. Solin, S. V. Naumov, V. G. Bamburov, N. I. Lobachevskaya, and O. G. Reznitskikh, Phys. Solid State. **41**, 262 (1999).
[21] M. Mozaffari, M. Eghbali Arani, and J. Amighian, J. Magn. Magn. Mater. **322**, 3240 (2010).